■ HIP

New insights into the biomechanics of Legg-Calvé-Perthes' disease

THE ROLE OF EPIPHYSEAL SKELETAL IMMATURITY IN VASCULAR OBSTRUCTION

M. Pinheiro,
C. A. Dobson,
D. Perry,
M. J. Fagan

University of Hull,
Kingston-upon-Hull,
United Kingdom

Objectives

Legg–Calvé–Perthes' disease (LCP) is an idiopathic osteonecrosis of the femoral head that is most common in children between four and eight years old. The factors that lead to the onset of LCP are still unclear; however, it is believed that interruption of the blood supply to the developing epiphysis is an important factor in the development of the condition.

Methods

Finite element analysis modelling of the blood supply to the juvenile epiphysis was investigated to understand under which circumstances the blood vessels supplying the femoral epiphysis could become obstructed. The identification of these conditions is likely to be important in understanding the biomechanics of LCP.

Results

The results support the hypothesis that vascular obstruction to the epiphysis may arise when there is delayed ossification and when articular cartilage has reduced stiffness under compression.

Conclusion

The findings support the theory of vascular occlusion as being important in the pathophysiology of Perthes disease.

Cite this article: *Bone Joint Res* 2018;7:148–156.

Keywords: Perthes' disease, Vessel obstruction, Juvenile hip, Biomechanics, Finite element analysis

■ M. Pinheiro, MEng, PhD, Medical and Biological Research Group,

■ C. A. Dobson, BSc(Hons), PhD, Medical and Biological Research Group,

■ M. J. Fagan, BSc(Hons), PhD, Medical and Biological Research Group, School of Engineering and Computer Science, University of Hull, Cottingham Road, Kingston-upon-Hull HU6 7RX, UK.

■ D. Perry, MB, ChB (Hons), FRCS (Orth), PhD, Institute of Translational Medicine, University of Liverpool, Crown Street, Liverpool L69 3BX, UK.

Correspondence should be sent to M. Pinheiro;
email: m.pinheiro@hull.ac.uk

Article focus

■ This article explores potential mechanisms of vascular occlusion within the epiphysis that may lead to Perthes' disease of the hip.

■ These mechanisms are investigated with a high-resolution finite element model of the juvenile hip incorporating the retinacular vessels

Key messages

■ Vascular obstruction at the epiphysis may arise when there is both delayed ossification and articular cartilage that has compromised compressive stiffness.

■ Initial obstruction of the blood supply may lead to alterations in bone properties, increasing the likelihood of further femoral head collapse.

■ A vascular mechanism for Perthes' disease seems possible in a child with skeletal immaturity, in combination with an acute cartilage insult.

Strengths and limitations

■ This study uses a unique high-resolution finite element model of the juvenile hip incorporating the retinacular vessels.

■ The study is hypothesis-generating, and experimental models of disease are required to formally test these hypotheses.

Introduction

Legg–Calvé–Perthes' disease (LCP or Perthes' disease) is an idiopathic osteonecrosis of the femoral head that most frequently occurs between four and eight years old.[1,2] Although described more than 100 years ago by four independent studies,[3-6] the aetiology of Perthes' disease remains poorly understood. LCP is between four and five times more common in boys than in girls, and children

with this disease have delayed skeletal development of between one and two years.[7,8] Approximately 90% of LCP cases are unilateral.[1] In the most severe cases, LCP can lead to the permanent flattening of the femoral head, articular cartilage degeneration and early osteoarthritis.[9]

An impairment or obstruction of the blood supply to the developing femoral head is thought to be the most likely mechanism for the disease. Factors leading to this vascular obstruction are unclear and are the subject to debate. During development, the epiphyseal blood supply is almost exclusively provided by the deep branch of the medial femoral circumflex artery (MFCA).[10] Both imaging and histological studies have shown a partial or complete loss of blood flow[11,12] and the development of ischaemic necrosis[13] of the femoral head in Perthes' disease. Furthermore, there is evidence of abnormal peripheral vasculature in children with LCP.[14]

We have previously proposed five mechanisms for the pathology of Perthes' disease,[15] and the implications for the morphology of the juvenile hip and the biomechanics of the hip joint.[16] From these we suggested that fracture and collapse of the femoral head, even in an immature epiphysis, is unlikely. We now hypothesize that morphological changes of the femoral head, together with an alteration in the mechanical properties of the epiphyseal cartilage, may cause compression or occlusion of the retinacular vessels. Using high-resolution finite element (FE) models, we have investigated the simulated forces acting on the MFCA under a number of experimental conditions to determine if this hypothesis is plausible.

Materials and Methods

FE modelling has being increasingly used for implant biomechanical optimization,[17,18] custom-implant development,[19,20] and tissue engineering.[21] We have previously developed an FE model of a healthy 7.9-year-old male hip from CT data.[19] Several variations of this healthy model were developed to understand the impact of hip morphology in the loading of the bony epiphysis. Delayed ossification was modelled by offsetting the normal epiphysis inwards by 2.3 mm according the method of Kitoh et al,[22] whereas the cartilage thickness of the femoral head was defined by offsetting the healthy epiphyseal surface outwards by 2.0 mm.[23] Static muscle optimization was performed in each model to determine the loading conditions across the hip. The thigh muscles were modelled with simplified lines of action (Fig. 1a), and the physiological cross-sectional areas (PCSA) scaled to a body weight (BW) of 23 kg.[24] Muscle forces were obtained by considering the 24 muscles acting around the hip, using non-linear optimization.[16] The model was optimized for single-leg stance and predicted a hip joint reaction forces (HJR) of 3.36 BW, which compares well with previously reported values for juvenile subjects.[25]

In this current work, two high-resolution FE submodels were derived from the original (normal) and offset models (Fig. 1b). The main retinacular vessels that branch from the MFCA into the developing epiphysis were included in these sub-models of the femoral head (Fig. 1c). Here, in addition to the delay in epiphyseal ossification, other types of joint tissue immaturities were evaluated. Biomechanical immaturity of the bony epiphysis was modelled with different bone volume density (bone volume divided by total volume; BV/TV) and associated mechanical properties, whereas the degree of cartilage maturation was modelled by varying its stiffness in compression. The loading conditions obtained with the full models were mapped onto the two higher-resolution sub-models (HRSM) to assess the likelihood of vessel constriction for each combination of epiphyseal ossification, BV/TV, and cartilage stiffness.

Both the full models and the sub-models were meshed using a voxel-based FE mesher that uses the isosurface stuffing algorithm,[26] and consisted of approximately 3.0 million and 5.0 million quadratic tetrahedral elements, respectively. The mechanical properties for cortical bone were derived from a series of compressive tests using bone from juvenile subjects (12 children with ages ranging between four and 15 years).[27] Thus, an elastic modulus (Young's modulus) $E_{cortical} = 11880\ MPa$ was used, with yield and ultimate strains of 1.11% and 2.31%, respectively. In addition to delayed ossification,[9] Perthes' patients may also have delayed bone and cartilage maturation. Different values of BV/TV[28] and cartilage stiffness were considered across the juvenile epiphysis. The BV/TV values considered were $\{0.06, 0.10, 0.19, 0.28\}$, which correspond to a trabecular bone apparent modulus $E_{trabecular}$ of:[29]

$$E_{trabecular} = 1.240\ E_{tissue} \left(\frac{BV}{TV} \right)^{1.8} \qquad (1)$$

where E_{tissue} was set equal to $E_{cortical}$. The corresponding Young's modulus for the target BV/TV values were then $E_{epiphysis} = \{100, 250, 750, 1500\}$ MPa, respectively. In the analysis, only the mechanical properties of the epiphysis were changed; the other trabecular bone properties were kept constant ($E_{trabecular} = 1500 MPa$). The articular cartilage modulus was also varied between the following values, $E_{cartilage} = \{0.50, 1.00, 1.50, 2.00\}$ MPa.

The geometry of the vessels was derived from an analysis of the anatomical descriptions found in the literature.[30,31] The MFCA and the three main retinacular vessels were modelled as solid tubular structures with an outer diameter of 1.60 mm and 0.80 mm, respectively, and included in the two HRSM (Fig. 1b). The properties of the retinacular vessels were derived from the literature.[32] Vessel obstruction was then assessed by comparing the loaded and unloaded cross-sectional areas of the retinacular vessels. The general shape of the distorted cross-sections was also assessed by computing the deviation of
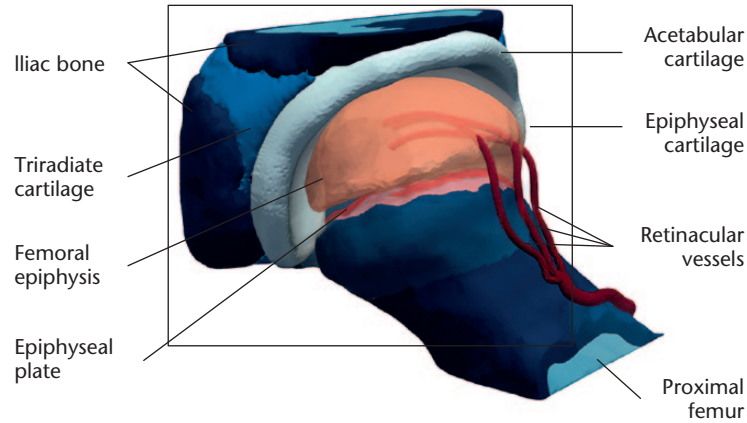
Fig. 1b

Fig. 1a

Fig. 1c

A full musculoskeletal model of the hip of a healthy 7.9-year-old male subject showing the muscle lines of action, with symmetry plane along the sagittal plane, described in a previous study by authors of this paper,[16] simulated in single-leg stance considering a healthy epiphysis and a small ossified epiphysis and different levels of bone and cartilage maturity. b) High-resolution computational model of the hip joint containing the three main superior retinacular vessels that constitute the main blood supply to the developing epiphysis. c) Photograph showing the superior retinacular arteries of the deep MFCA (adapted from **Lazaro LE, Klinger CE, Sculco PK, Helfet DL, Lorich DG.** The terminal branches of the medial femoral circumflex artery: the arterial supply of the femoral head. *Bone Joint J* 2015;97-B:1204-1213.)[29] and the computer-aided design model of three main superior retinacular arteries.

Table I. Material properties considered in the juvenile hip model[16,32]

Material properties	Cortical bone	Trabecular bone	Epiphyseal plate	Epiphyseal cartilage	Pubic symphysis	Acetabular labrum	Retinacular vessels
Young's modulus (MPa)	11 880	100 to 1500	0.75	0.50 to 2.00	5.00	5.00	0.11
Poisson's ratio	0.300	0.300	0.495	0.495	0.450	0.495	0.490

the outer cross-sectional geometry from the (ideal) circular shape through the elliptical eccentricity index:

$$r = \sqrt{1 - \frac{b^2}{a^2}} \qquad (2)$$

where $0 \leq r \leq 1$ is a dimensionless parameter (with $r = 0$ for a circle), and a and b are the lengths of the semi-major and the semi-minor axis of the ellipse, respectively. According to Shilo and Gefen,[33] who studied capillary behaviour under large compressive and shear tissue deformations, complete collapse of blood vessels occurs when $r \geq 0.88$. The Young's modulus and Poisson's ratio of the vessels were assumed to be $E_{vessel} = 0.11 MPa$ and $v = 0.490$, respectively.

All materials were modelled as linear elastic, isotropic and homogenous, and all model simulations were carried out in ANSYS v15 (ANSYS Inc., Canonsburg, Pennsylvania). The full details of the material properties used are summarized in Table I. The ultimate strain for the trabecular bone was defined as 2.31% and considered constant across different BV/TV. Equivalence between the loading of the two models was obtained by mapping the nodal displacements from the full to the HRSM.

This research was part of a larger study investigating the diagnosis and prevention of Perthes' disease. Ethical approval for the work was given by the Office for Research Ethics Committees Northern Ireland (ORECNI), REF 13/NI/0139.
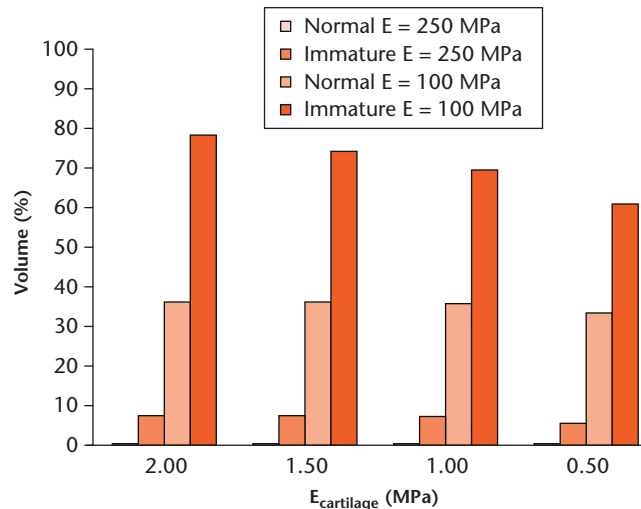
Fig. 2

Proportion of the epiphyseal volume above the ultimate strain (2.31%) in the healthy (normal) and immature femoral head for $E_{epiphysis} \geq 250$ MPa (BV/TV=0.10) and $E_{epiphysis} = 100$ MPa (BV/TV=0.06) with different cartilage properties. (Values for E=250MPa are <0.1%)

Results

Both the full model and sub-model of the developing femoral epiphysis were simulated under single-leg stance. The strain values across the bony epiphysis were uniformly very low, and only for low BV/TV values were there significant portions of the femoral epiphysis above the ultimate strain. Figure 2 shows the proportion of epiphyseal volume above the ultimate strain of 2.31%, for healthy and sample immature models with $\frac{BV}{TV} = \{0.06, 0.10\}$, considering different cartilage properties. In the immature epiphysis, the volume above the ultimate strain is up to 7.3% of the overall ossified volume for $E_{epiphysis} = 250$ MPa. For a BV/TV = 0.06 both the healthy and immature epiphysis have a higher percentage of bone volume above the ultimate strain (up to 36% for the healthy epiphysis and between 60.7% and 78.3 % for the immature epiphysis).

Figures 3a and 3b presents the displacement of the femoral head with healthy and immature proximal femoral epiphysis with $E_{epiphysis} = 1500$ MPa and $E_{cartilage} = 0.50$ MPa. In the healthy epiphysis, the overall shape of the epiphysis is preserved. A softer epiphyseal cartilage leads to an increase in its lateral displacement; nevertheless, this is limited by the ossified epiphysis (Fig. 3a). In contrast, in the small/skeletally immature head, there is more lateral displacement of the cartilage, and this becomes more pronounced as the stiffness of the cartilage decreases (Fig. 3b).

The lateral displacement of the cartilage causes the blood vessels to be stretched as they pass through the articular cartilage (Fig. 3b). For a small epiphysis, reducing the stiffness of the articular cartilage leads to an increase in the lateral displacement and stretching of the blood vessels, irrespective of the bone density of the femoral epiphysis (all models are shown in supplementary Fig. a). Table II and Table III list the minimum and

maximum displacements for each combination of $E_{epiphysis}$ and $E_{cartilage}$ for the healthy and small femoral epiphysis, respectively. For instance, for the healthy epiphysis and a $E_{epiphysis} = 1500$ MPa, vessel displacement remains relatively unchanged as the stiffness of the cartilage is reduced (with a maximum vessel stretch of 1.12 mm for $E_{cartilage} = 0.50$ MPa, Table II and supplementary Fig. b), whereas for the small epiphysis and $E_{cartilage} = 0.50$ MPa the blood vessel stretch is 2.75 mm (Table III and Fig. a). The vessel cross-sectional distortion also increases (Table IV) and the cross-sectional area decreases (Table V) as cartilage becomes softer. For $E_{cartilage} \leq 1.0$ MPa there is an almost complete collapse of the blood vessels (with r ≈ 0.88), whereas the reduction in the cross-sectional area ranges from approximately 22% to 68%. Figure 4 shows the change in the cross-sections of the three blood vessels (anterior, medial, and posterior) across the regions of highest distortion. Vessel twisting was also observed, especially in the posterior vessel (Figs 4a to 4d).

Discussion

We have shown that significant vessel obstruction can occur when there is delayed ossification of the bony epiphysis and reduced stiffness of the articular cartilage, under simple single-leg stance loading conditions. The obstruction of the blood supply may lead to further reduction in bone and articular cartilage biomechanical properties, increasing the likelihood of further femoral head collapse.

Under the loading conditions considered, collapse of the femoral epiphysis due to overload is unlikely to occur, unless the BV/TV of the trabecular bone is extremely low (Fig. 2). Overloading occurs for very low values of $BV / TV = 0.06$, which corresponds to a skeletal immaturity greater than the one to two years normally observed
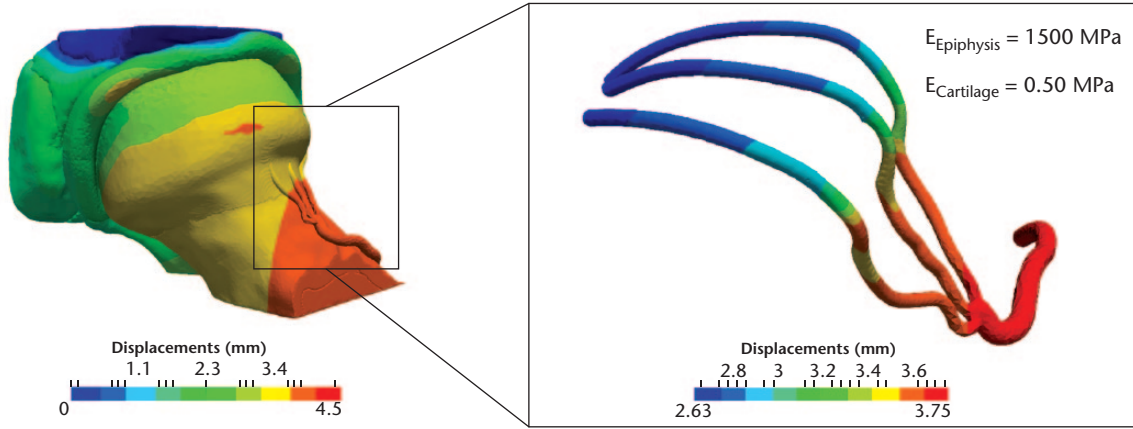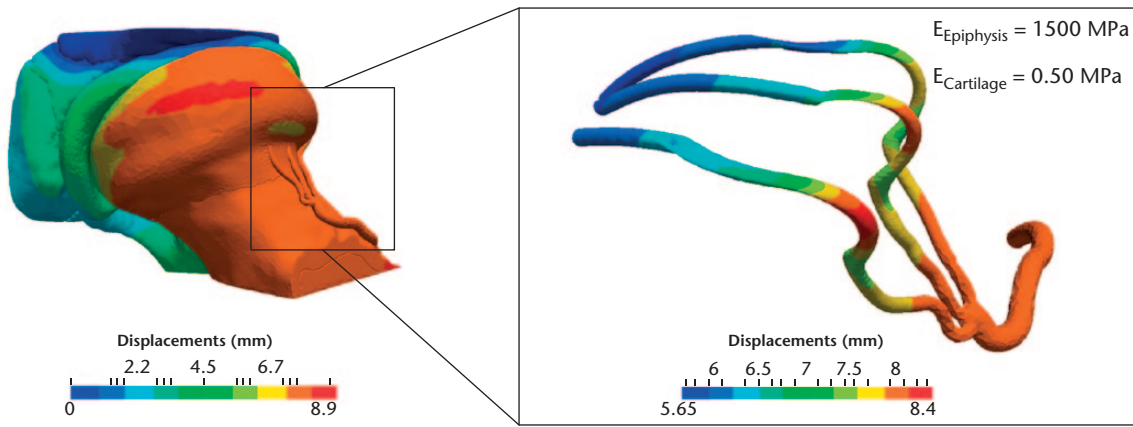
Fig. 3a

Fig. 3b

Displacements of the juvenile hip and three main terminal branches of the deep MFCA for a) the healthy femoral epiphysis with $E_{epiphysis}$ = 1500 MPa and $E_{cartilage}$=0.50 MPa, and b) the skeletally immature epiphysis with $E_{epiphysis}$ = 1500 MPa and $E_{cartilage}$=0.50 MPa.

Table II. Minimum and maximum blood vessel displacements (mm) as a function of $E_{epiphysis}$ and $E_{cartilage}$ with the healthy epiphysis (see supplementary information Fig. b)

$E_{epiphysis}$ (MPa)	BV/TV	$E_{cartilage}$ (MPa) 2.00, range	$E_{cartilage}$ (MPa) 1.50, range	$E_{cartilage}$ (MPa) 1.00, range	$E_{cartilage}$ (MPa) 0.50, range
1500	0.28	1.55 to 2.50	1.73 to 2.72	2.02 to 3.06	2.63 to 3.75
750	0.19	1.55 to 2.51	1.73 to 2.73	2.02 to 3.08	2.63 to 3.77
250	0.10	1.55 to 2.57	1.73 to 2.78	2.03 to 3.13	2.63 to 3.81
100	0.06	1.56 to 2.68	1.74 to 2.90	2.04 to 3.24	2.64 to 3.92

Table III. Minimum and maximum blood vessel displacements (mm) as a function of $E_{epiphysis}$ and $E_{cartilage}$ with the small/immature epiphysis (see supplementary information Fig. a)

$E_{epiphysis}$ (MPa)	BV/TV	$E_{cartilage}$ (MPa) 2.00, range	$E_{cartilage}$ (MPa) 1.50, range	$E_{cartilage}$ (MPa) 1.00, range	$E_{cartilage}$ (MPa) 0.50, range
1500	0.28	2.84 to 4.46	3.29 to 5.03	4.04 to 6.07	5.65 to 8.40
750	0.19	2.82 to 4.47	3.27 to 5.04	4.03 to 6.08	5.68 to 8.41
250	0.10	2.76 to 4.51	3.20 to 5.08	3.96 to 6.12	5.67 to 8.45
100	0.06	2.69 to 4.58	3.12 to 5.15	3.86 to 6.19	5.55 to 8.51

in LCP patients.[34] These observations support the results of our previous work.[16] Even with such significantly reduced bone stiffness, only 7.3% of the epiphysis was overloaded.

Table IV. Cross-sectional eccentricity (r) of each retinacular vessel as they pass through the epiphyseal cartilage for the skeletally immature epiphysis (BV/TV values for the trabecular bone displayed in brackets)

$E_{epiphysis}$ (MPa)	$E_{cartilage}$ (MPa) 2.00			$E_{cartilage}$ (MPa) 1.50			$E_{cartilage}$ (MPa) 1.00			$E_{cartilage}$ (MPa) 0.50		
	Ant.	Med.	Pos.	Ant.	Med.	Pos.	Ant.	Med.	Pos.	Ant.	Med.	Pos.
1500 (0.28)	0.72	0.74	0.73	0.78	0.80	0.78	0.85	0.87	0.84	0.94	0.96	0.92
750 (0.19)	0.72	0.75	0.74	0.78	0.80	0.79	0.85	0.87	0.85	0.94	0.96	0.93
250 (0.10)	0.72	0.75	0.76	0.78	0.80	0.81	0.85	0.87	0.86	0.94	0.96	0.94
100 (0.06)	0.73	0.75	0.79	0.79	0.80	0.83	0.86	0.87	0.89	0.94	0.96	0.95

ant., anterior; med., medial; pos., posterior

Table V. Variation of the cross-sectional area (%) for each retinacular vessel as they pass through the epiphyseal cartilage for the skeletally immature epiphysis (BV/TV values for the trabecular bone displayed in brackets)

$E_{epiphysis}$ (MPa)	$E_{cartilage}$ (MPa) 2.00			$E_{cartilage}$ (MPa) 1.50			$E_{cartilage}$ (MPa) 1.00			$E_{cartilage}$ (MPa) 0.50		
	Ant.	Med.	Pos.	Ant.	Med.	Pos.	Ant.	Med.	Pos.	Ant.	Med.	Pos.
1500 (0.28)	-21.9	-22.2	-13.9	-26.1	-28.2	-19.1	-32.9	-39.4	-21.6	-45.5	-67.7	-31.6
750 (0.19)	-21.9	-22.1	-14.8	-26.1	-28.1	-17.9	-32.8	-39.3	-22.7	-45.5	-67.6	-32.7
250 (0.10)	-21.8	-21.8	-17.2	-26.0	-27.8	-20.7	-32.7	-38.9	-26.0	-45.5	-67.3	-36.6
100 (0.06)	-21.8	-21.2	-20.0	-26.1	-27.2	-24.1	-32.8	-38.2	-30.5	-45.9	-66.6	-42.8

ant., anterior; med., medial; pos., posterior

In an MRI study of adults, it was found that necrosis of more than 30% of the epiphyseal volume was necessary to cause the collapse of the femoral head.[35] In a similar radiological study, it was found that femoral head collapse depended on the size of the necrotic region and its position relative to the medial weight-bearing area but, for example, a failure rate of only 4.5% was reported for necrotic volumes < 30%.[36]

For a healthy epiphysis, vessel distortion was negligible irrespective of the BV/TV and cartilage stiffness values considered (Fig. 3a), whereas for a small epiphysis, significant vessel distortion was observed even for moderately reduced levels of cartilage stiffness (Fig. 3b; Tables III and IV). Hence, the combination of epiphyseal size and stiffness of the cartilage has a more critical impact on vessel constriction than bone maturation (reflected by BV/TV) in our modelling.

An early study in LCP suggested that damage to the articular cartilage might precede the degeneration of the secondary ossification centre.[37] Ischaemic-induced necrosis of the femoral epiphyses in piglets has also been shown to cause both structural changes often observed in LCP,[38] as well as the injury to the deep layer of epiphyseal cartilage around the secondary ossification centre.[39] Kim et al[40] observed that the biomechanical properties of cartilage and bone significantly decrease in the infarcted femoral head. These changes to both bone and cartilage of the developing femoral head have been modelled in this study. We have demonstrated that vascular obstruction may occur from a combination of delayed ossification and reduced stiffness of the articular cartilage. The results suggest that cartilage injury and growth arrest may be established prior to the occlusion of the MFCA for Perthes' disease to develop. Both factors, independently,

seem to be insufficient to cause the collapse of the retinacular vessels.

Both the FE models investigated included several simplifications. For loading, the muscles were simplified to single lines of action.[16] All materials were modelled as homogeneous with linear elastic properties, which is a simplification of the more complex non-isotropic and nonlinear behaviour of both bone and cartilage. Finally, the retinacular vessels' dimensions and overall geometry were taken from a single X-ray study[31] The modelled vessels may not accurately represent the juvenile MFCA and retinacular vessels. The vessel diameter was kept constant (0.80 mm) for the three retinacular arteries, which may be slightly oversized compared to other values reported for juvenile subjects.[30,31] Despite these simplifications, the results are still interesting and provide useful insights into the potential mechanisms that could lead to LCP.

The underlying cause of reduced cartilage stiffness is unclear. During maturation of articular cartilage, there is known to be an increase in tensile and compressive stiffness.[41] Proteoglycan and collagen fibres are the major contributors to stiffness under compression.[42] Any variation in collagen or proteoglycan makeup will affect the biomechanical properties. Cartilage injury may release proteoglycan fragments into the synovial fluid[43] and has been reported in LCP. The macroscopic modulus of degenerative articular cartilage has been found to be as low as 0.28 MPa to 0.50 MPa in adult osteoarthritic joints.[44] In the current study, values of 0.50 MPa and 1.00 MPa were found to lead to reductions in vessel cross-sectional area of 68% and 40% respectively, during single-leg stance, which is a normal loading pattern. Articular cartilage injury and release of degradation products into the synovial fluid has a synergistic effect on the
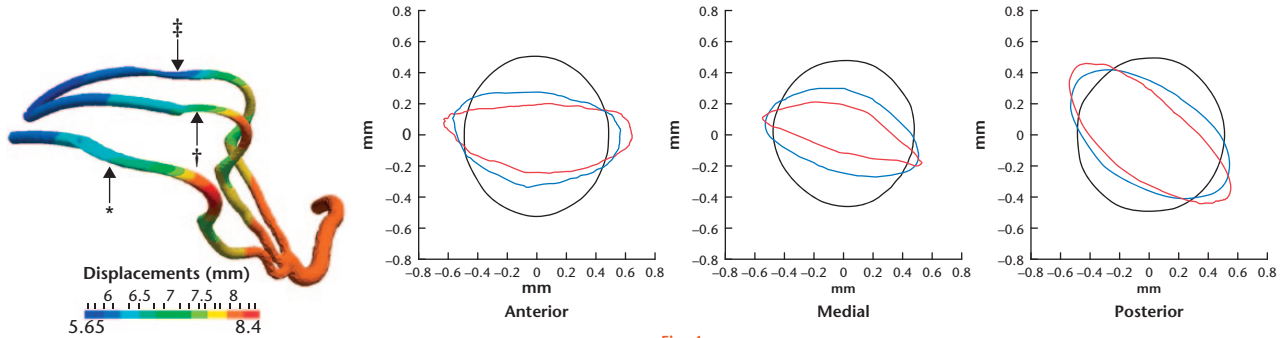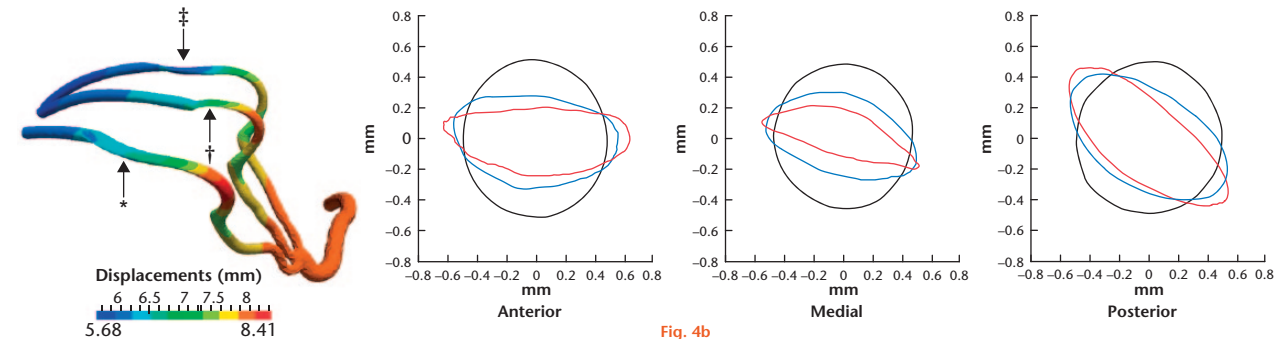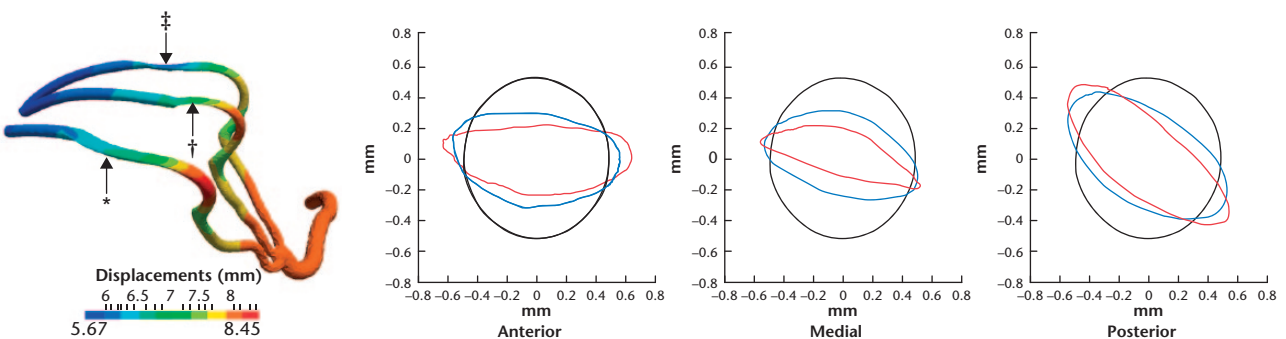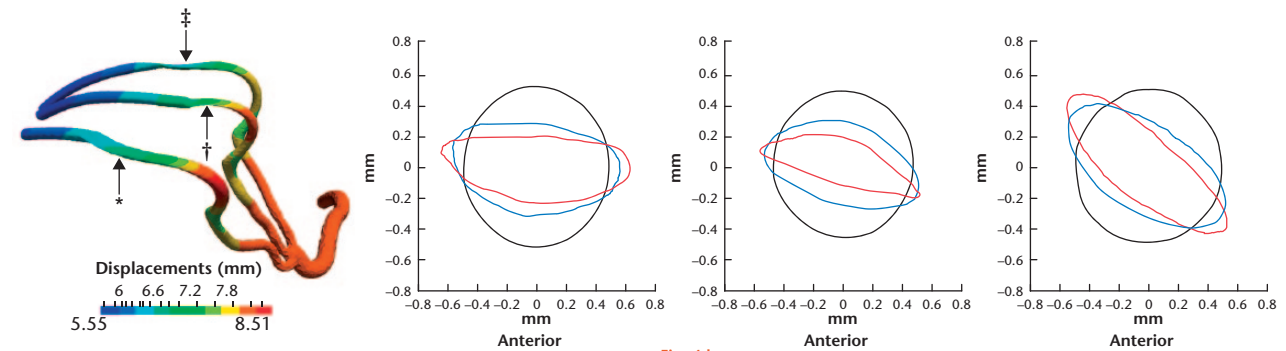
Fig. 4a

Fig. 4b

Fig. 4c

Fig. 4d

Displacement of the blood vessels in the immature epiphysis and vessel critical cross-sections for the undeformed (black) and deformed anterior (*), medial (†), and posterior (‡) retinacular arteries, for $E_{cartilage} = 1.00$ MPa (blue) and $E_{cartilage} = 0.50$ MPa (red): a) $E_{epiphysis} = 1500$ MPa, b) $E_{epiphysis} = 750$ MPa, c) $E_{epiphysis} = 250$ MPa, and d) $E_{epiphysis} = 100$ MPa.

inflammatory response of the synovium, causing further cartilage breakdown, joint effusion, stiffness, and pain.[45]

While this study explores the potential mechanisms Perthes disease, the aetiology remains uncertain. One possible explanation that could fit the hypothesized mechanism combines delayed development and transient synovitis. Skeletal immaturity or 'skeletal standstill' is well described in Perthes' disease and this may be

related to societal exposures, such as worsening socio-economic deprivation.[46] An at risk skeletally immature hip may then suffer a relatively benign injury to the cartilage, and through a process such as transient synovitis,[47] these events may be enough to precipitate the onset of LCP through vascular occlusion.

The two high-resolution finite element models of the juvenile hip suggest that significant vessel obstruction can occur when there is delayed ossification of the femoral head epiphysis and there is reduced stiffness of the articular cartilage, under simple single-leg stance loading. The continued obstruction of the blood supply may lead to further reduction in bone stiffness and strength, increasing the likelihood of progressive femoral head collapse.

Supplementary material

Figures showing the displacements of the blood vessels for values of trabecular bone Young's modulus and cartilage stiffness for the normal and immature epiphysis are available alongside this article at www.bjr.boneandjoint.org.uk

References

1. **Perry DC, Skellorn PJ, Bruce CE.** The lognormal age of onset distribution in Perthes' disease: an analysis from a large well-defined cohort. *Bone Joint J* 2016;98-B:710-714.
2. **Perry DC, Thomson C, Pope D, Bruce CE, Platt MJ.** A case control study to determine the association between Perthes' disease and the recalled use of tobacco during pregnancy, and biological markers of current tobacco smoke exposure. *Bone Joint J* 2017;99-B:1102-1108.
3. **Waldenström H.** Der obere tuberkulose collumherd. *Zeitschrf Orthop Chir* 1909;24:487-512. (in German)
4. **Legg AT.** An obscure affection of the hip-joint. *Bost Med Surg J Massachusetts Medical Society* 1910;162:202-204.
5. **Calvé J.** Sur une forme particulière de pseudo-coxalgie greffée sur des déformations caractéristiques de l'extrémité supérieure du fémur. *Rev Chir* 1910;42:54-84. (in French)
6. **Perthes G.** Über Arthritis deformans juvenilis. *Deutsch Zeitschr Chir* 1910;107:111-159. (in German)
7. **Chaudhry S, Phillips D, Feldman D.** Legg-Calvé-Perthes disease: an overview with recent literature. *Bull Hosp Jt Dis* (2013) 2014;72:18-27.
8. **Shohat N, Gilat R, Shitrit R, et al.** A long-term follow-up study of the clinical and radiographic outcome of distal trochanteric transfer in Legg-Calvé-Perthes' disease following varus derotational osteotomy. *Bone Joint J* 2017;99-B:987-992.
9. **Kim HKW, Herring JA.** Legg-Calvé-Perthes' disease. In: Herring JA, ed. *Tachdjian's Pediatric Orthopaedics: From the Texas Scottish Rite Hospital for Children*. Fifth ed. Vol. 1. Philadelphia: Elsevier, 2014:580-629.[[bibmisc]]
10. **Trueta J.** The normal vascular anatomy of the human femoral head during growth. *J Bone Joint Surg [Br]* 1957;39-B:358-394.
11. **Lamer S, Dorgeret S, Khairouni A, et al.** Femoral head vascularisation in Legg-Calvé-Perthes disease: comparison of dynamic gadolinium-enhanced subtraction MRI with bone scintigraphy. *Pediatr Radiol* 2002;32:580-585.
12. **Kim HKW, Kaste S, Dempsey M, Wilkes D.** A comparison of non-contrast and contrast-enhanced MRI in the initial stage of Legg-Calvé-Perthes disease. *Pediatr Radiol* 2013;43:1166-1173.
13. **Jonsater S.** Coxa plana; a histo-pathologic and arthrografic study. *Acta Orthop Scand Suppl* 1953;12:5-98.
14. **Perry DC, Green DJ, Bruce CE, et al.** Abnormalities of vascular structure and function in children with Perthes disease. *Pediatrics* 2012;130:e126-e131.
15. **Berthaume MA, Perry DC, Dobson CA, et al.** Skeletal immaturity, rostral sparing, and disparate hip morphologies as biomechanical causes for Legg-Calvé-Perthes' disease. *Clin Anat* 2016;29:759-772.
16. **Pinheiro M, Dobson CA, Clarke NM, Fagan MJ.** The potential role of variations in juvenile hip geometry on the development of Legg-Calvé-Perthes disease: a biomechanical investigation [accepted for publication in Computer Methods in Biomechanics and Biomedical Engineering].

17. **Scott CEH, Eaton MJ, Nutton RW, et al.** Metal-backed versus all-polyethylene unicompartmental knee arthroplasty: proximal tibial strain in an experimentally validated finite element model. *Bone Joint Res* 2017;6:22-30.
18. **Nakamura S, Tian Y, Tanaka Y, et al.** The effects of kinematically aligned total knee arthroplasty on stress at the medial tibia: A case study for varus knee. *Bone Joint Res* 2017;6:43-51.
19. **Pinheiro M, Alves JL.** A new level-set based protocol for accurate bone segmentation from CT imaging. *IEEE Access* 2015;3:1894-1906.
20. **Pinheiro M, Alves JL.** The feasibility of a custom-made endoprosthesis in mandibular reconstruction: implant design and finite element analysis. *J Craniomaxillofac Surg* 2015;43:2116-2128.
21. **Castro APG, Lacroix D.** Micromechanical study of the load transfer in a polycaprolactone-collagen hybrid scaffold when subjected to unconfined and confined compression. *Biomech Model Mechanobiol* 2017. (Epub ahead of print) PMID: 29129026
22. **Kitoh H, Kitakoji T, Katoh M, Takamine Y.** Delayed ossification of the proximal capital femoral epiphysis in Legg-Calvé-Perthes' disease. *J Bone Joint Surg [Br]* 2003;85-B:121-124.
23. **Castriota-Scanderbeg A, De Micheli V.** Ultrasound of femoral head cartilage: a new method of assessing bone age. *Skeletal Radiol* 1995;24:197-200.
24. **Lappin K, Kealey D, Cosgrove A, Graham K.** Does low birthweight predispose to Perthes' disease? Perthes' disease in twins. *J Pediatr Orthop B* 2003;12:307-310.
25. **Carriero A, Zavatsky A, Stebbins J, et al.** Influence of altered gait patterns on the hip joint contact forces. *Comput Methods Biomech Biomed Engin* 2014;17:352-359.
26. **Labelle F, Shewchuk J.** Isosurface stuffing: fast tetrahedral meshes with good dihedral angles. *ACM Trans Graph* 2007;26:1-10.
27. **Öhman C, Baleani M, Pani C, et al.** Compressive behaviour of child and adult cortical bone. *Bone* 2011;49:769-776.
28. **Parfitt AM, Travers R, Rauch F, Glorieux FH.** Structural and cellular changes during bone growth in healthy children. *Bone* 2000;27:487-494.
29. **Yang G, Kabel J, van Rietbergen B, et al.** The anisotropic Hooke's law for cancellous bone and wood. *J Elast* 1998;53:125-146.
30. **Lazaro LE, Klinger CE, Sculco PK, Helfet DL, Lorich DG.** The terminal branches of the medial femoral circumflex artery: the arterial supply of the femoral head. *Bone Joint J* 2015;97-B:1204-1213.
31. **Tucker FR.** Arterial supply to the femoral head and its clinical importance. *J Bone Joint Surg [Br]* 1949;31-B:82-93.
32. **Hunter KS, Albietz JA, Lee P-F, et al.** In vivo measurement of proximal pulmonary artery elastic modulus in the neonatal calf model of pulmonary hypertension: development and ex vivo validation. *J Appl Physiol (1985)* 2010;108:968-975.
33. **Shilo M, Gefen A.** Identification of capillary blood pressure levels at which capillary collapse is likely in a tissue subjected to large compressive and shear deformations. *Comput Methods Biomech Biomed Engin* 2012;15:59-71.
34. **Ryan TM, Krovitz GE.** Trabecular bone ontogeny in the human proximal femur. *J Hum Evol* 2006;51:591-602.
35. **Nishii T, Sugano N, Ohzono K, et al.** Significance of lesion size and location in the prediction of collapse of osteonecrosis of the femoral head: a new three-dimensional quantification using magnetic resonance imaging. *J Orthop Res* 2002;20:130-136.
36. **Lieberman JR, Engstrom SM, Meneghini RM, SooHoo NF.** Which factors influence preservation of the osteonecrotic femoral head? *Clin Orthop Relat Res* 2012;470:525-534.
37. **Ponseti IV, Maynard JA, Weinstein SL, Ippolito EG, Pous JG.** Legg-Calvé-Perthes disease. Histochemical and ultrastructural observations of the epiphyseal cartilage and physis. *J Bone Joint Surg [Am]* 1983;65-A:797-807.
38. **Shapiro F, Connolly S, Zurakowski D, et al.** Femoral head deformation and repair following induction of ischemic necrosis: a histologic and magnetic resonance imaging study in the piglet. *J Bone Joint Surg [Am]* 2009;91-A:2903-2914.
39. **Kim HKW, Su PH, Qiu YS.** Histopathologic changes in growth-plate cartilage following ischemic necrosis of the capital femoral epiphysis. An experimental investigation in immature pigs. *J Bone Joint Surg [Am]* 2001;83-A:688-697.
40. **Koob TJ, Pringle D, Gedbaw E, et al.** Biomechanical properties of bone and cartilage in growing femoral head following ischemic osteonecrosis. *J Orthop Res* 2007;25:750-757.
41. **Asanbaeva A, Tam J, Schumacher BL, et al.** Articular cartilage tensile integrity: modulation by matrix depletion is maturation-dependent. *Arch Biochem Biophys* 2008;474:175-182.
42. **Sophia Fox AJ, Bedi A, Rodeo SA.** The basic science of articular cartilage: structure, composition, and function. *Sports Health* 2009;1:461-468.
43. **Lohmander LS, Wingstrand H, Heinegård D.** Transient synovits of the hip in the child: increased levels of proteoglycan fragments in joint fluid. *J Orthop Res* 1988;6:420-424.

44. **Kleemann RU, Krocker D, Cedraro A, Tuischer J, Duda GN.** Altered cartilage mechanics and histology in knee osteoarthritis: relation to clinical assessment (ICRS Grade). *Osteoarthritis Cartilage* 2005;13:958-963.

45. **Sellam J, Berenbaum F.** The role of synovitis in pathophysiology and clinical symptoms of osteoarthritis. *Nat Rev Rheumatol* 2010;6:625-635.

46. **Burwell RG.** Perthes' disease: growth and aetiology. *Arch Dis Child* 1988;63:1408-1412.

47. **Harrison WD, Vooght AK, Singhal R, Bruce CE, Perry DC.** The epidemiology of transient synovitis in Liverpool, UK. *J Child Orthop* 2014;8:23-28.